Amorphous carbon films deposited from carbon ions extracted from a discharge in fullerene vapor

E. B. Maiken[a] and P. Taborek
Department of Physics and Astronomy, University of California, Irvine, California 92697

(Received 5 November 1998; accepted for publication 4 January 2000)

Amorphous carbon (*a*-C) films with physical properties ranging from diamond like to graphite like were deposited at rates of 1 μm/h under 10^{-6} Torr vacuum by extracting a molecular carbon ion beam from a pure carbon discharge in fullerene vapor. With ion energies fixed near 300 eV, substrate temperature and beam neutralization were the main process parameters controlling film properties. *a*-C stress and density increased with decreasing deposition temperature, ranging to greater than 3 GPa and 2.9 g/cm^3, respectively. Room temperature conductivity ranged from 10 to $10^{-11}(\Omega\ \mathrm{cm})^{-1}$, with cool substrates and a well neutralized ion beam producing the most insulating films. *a*-C conductivity increased irreversibly after imposition of electric fields exceeding 10^8 V/m through the film planes. The high conductivities of films deposited without a beam neutralizer are attributed to phase changes resulting from dielectric breakdown driven by electric fields induced by surface charging. Conductivity data obtained for films deposited at different temperatures are discussed in the context of activated conduction, variable range hopping, and multiphonon assisted hopping transport processes. © *2000 American Institute of Physics.*
[S0021-8979(00)04707-1]

I. INTRODUCTION

The past decade's explosion of fullerene research has dominated studies of the wide range of solids arising from the multiple bonding hybridizations available to carbon atoms. Although fullerene materials science has emphasized formulation of complex derivatives of the archetypal C_{60}, investigations of dissociation mechanisms[1,2] have paralleled the use of decomposed fullerenes as carbon feedstock for the deposition of amorphous carbon[2–7] and diamond.[8] Concurrent studies of hydrogen-free amorphous carbon (*a*-C)[9] films deposited from nonfullerene precursors have been driven by both fundamental inquiries and by the utility of coatings that approach the superlative physical characteristics of bulk diamond. Integrating these areas of research, we extend our previous work[3,4] by detailing modifications of our fullerene based *a*-C deposition process and reporting bulk material data for a wide range of a *a*-C films. Our ion beam process is distinct from other plasma,[8] neutral-beam,[5] and ion-beam[2,6,7] deposition methods employing vaporized fullerenes because we decomposed the fullerenes in a discharge that was remote from the substrate and because no other gasses, such as argon or hydrogen, were used during depositions. Additionally, our use of a gridded broad beam ion source allowed independent control of ion flux and energy while permitting a scaleup to depositions over large areas. The density, intrinsic stress, and temperature dependence of the conductivity of *a*-C films deposited at different substrate temperatures were measured. The *a*-C properties ranged from hard, insulating diamond-like carbon to soft, conductive graphite-like carbon, with no evidence of residual intact fullerene material.[3] The properties of the films are therefore discussed within the context of an amorphous covalent material rather than as a fullerene molecular solid.

II. EXPERIMENTAL DETAILS

The experimental details are divided into Secs. II A and II B, beginning with a description of modifications made to the fullerene-based *a*-C deposition process since our last report.[3] This new material includes consideration of the effects of ion beam neutralization and use of an expanded range of deposition temperatures. We then describe *in situ* measurements of the temperature dependence of the *a*-C electrical conductivity and *ex situ* measurements of the film bulk density and stress.

A. Amorphous carbon deposition

We constructed a specialized ion source that dissociated vaporized fullerenes into small ionized and neutral carbon clusters.[3] The oscillating electron ion gun was designed to use a solid state fullerene feedstock, with special features including an integral crucible and construction from refractory materials to allow operation at temperatures of up to 900 K, which minimized fullerene vapor condensation on the graphite electrodes. The source was heated by an internal hot cathode and by thermal contact with the resistively heated crucible. A schematic diagram of the deposition system is shown in Fig. 1. Prior to depositions, the fullerene-filled crucible, ion gun, and substrate were baked under vacuum for several hours at 300 °C to remove sources of hydrogen such as organic solvents or water. Substrates were then sputter cleaned by a 500 eV Ar ion beam produced by a commercial broad beam source. A beam of molecular carbon ions, comprised of approximately 2–6 atoms each,[3] was ex-

[a]Present address: N&K Technology, Inc., 3150 DeLa Cruz Blvd., Santa Clara, CA 95054; electronic mail: emaiken@nandk.com

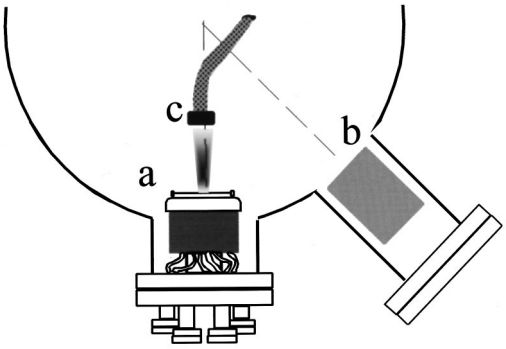

FIG. 1. Diagram of the system used for *a*-C deposition and conductivity measurement. Prior to depositions, the substrate (c) was sputtered using the broad beam ion source (b). A 1 cm^2 diam carbon ion beam, extracted from the ceramic source (a), impinged upon the substrate (c). After depositions, *a*-C conductivity was measured using the substrate holder to control and monitor temperature.

tracted from the fullerene discharge, focused, and accelerated by grids. The beam was directed onto the substrate, where the carbon ions energetically condensed into an *a*-C film. Depositions were made under 10^{-6} Torr vacuum, with *a*-C growth rates of approximately l μm/h, monitored by a quartz crystal. Controllable carbon ion source parameters included fullerene vapor pressure, discharge current, beam current, beam neutralization, and ion energy. Deposition temperature was monitored by a thermocouple clamped to the substrate, and determined by the balance between heating by ion impact and source radiation, and conduction to the copper substrate holder, which could be cooled by liquid nitrogen or heated by an embedded filament. After depositions, the substrate holder was used to control the *a*-C temperature during *in situ* conductivity measurements. A series of *a*-C films was produced for this study under identical ion source settings, with 6 min depositions resulting in nominally 0.1 μm thick films. Film thicknesses were determined by normal reflectance interference fringes, by calibrating against surface profilometer measurements.

Because the *a*-C conductivity and optical absorption increased with higher deposition temperatures,[3] use of an external hot wire beam neutralizer was initially avoided to minimize radiative heating of the nearby substrate. However, with other parameters fixed, it was found that depositions with a neutralizer decreased *a*-C conductivity by many orders of magnitude compared to deposition with a non-neutralized beam. The ion beam was neutralized by adjusting the electron emission of a hot tungsten filament immersed in the beam for zero net current between the substrate and ground. For non-neutralized beams, positive carbon ions of charge q_{ion} impacted the substrate at an energy $E_{\text{ion}} = q_{\text{ion}}(V_P - V_S)$ determined by the ion source plasma bias V_P and the growing *a*-C film's front-face potential V_S.[3] Neglecting the ejected secondary electron current,[10] an estimate of the magnitude of V_S was obtained by considering that an insulating film with conductivity $\sigma_{\text{film}} = 10^{-10}\,\Omega^{-1}\,\text{cm}^{-1}$ and thickness $t \sim 10$ nm, under a typical ion current density j of 0.1 mA/cm^2, floated at $V_S = jt/\sigma_{\text{film}} \cong +1$ V. Hence, with V_P near +300 V, it was expected that a negligible decrement of the ion beam deposition energy occurred. However, as will be discussed in Sec. III A, the $\sim 10^8$ V/m electric field within the film would be comparable to field strengths that were observed to irreversibly increase *a*-C conductivity. The properties of growing films were also indirectly affected by the ion source discharge current I_D, which determined the distribution of molecular carbon ions extracted from the source. Increasing discharge currents resulted in a trend of fewer atoms per extracted ion, with average kinetic energy per deposited carbon atom of approximately 50–150 eV for $I_D = 0.5$ A.[3] Use of the beam neutralizer allowed depositions at well-defined ion energies by varying the discharge potential V_p. However, E_{ion} was held fixed at 300 eV because of the ambiguity of the energy per carbon atom resulting from the range of ion masses in the unfiltered beam.

B. Amorphous carbon bulk properties

The temperature dependence of the *a*-C dark conductivity was measured *in situ*, under vacuum, immediately following deposition on a glass substrate by either two or four point techniques. Measurements were made along the planes of conductive films and through highly insulating films, with both techniques yielding identical results for a test on a 0.1 μm thick conductive film. The planar electrode spacing was approximately 100 μm, while contacts for sandwich structures were separated by the nominal 0.1 μm film thicknesses. In all cases, the physical spacings were used for calculating the conductivity, with no correction for space charge layers. Contacts were made from sputter-cleaned and freshly evaporated gold electrodes. *Ex situ* photoelectron spectroscopy measurements placed the valence band of highly conducting *a*-C 5.1 eV below the vacuum. The relatively deep level was approximately midway between the 4.2 eV valance band measured for amorphous carbon deposited by pyrolysis of toluene and the 6.2 eV highest occupied molecular orbital (HOMO) level measured for evaporated C_{60} fullerenes. This indicates that a mixture of bond hybridizations were likely present in the *a*-C. Because the *a*-C valence band level was close to the work function for the gold contacts, the gold was expected to be an efficient hole injector, and the low field conductivity data may therefore be associated with hole transport. Nonetheless, no determinations of carrier type, density, or mobility were made.

A flotation technique was used to measure the bulk density of *a*-C films deposited without a beam neutralizer. After deposition, carbon flakes were removed from the substrate and placed in a vial with a few hundred microliters of a relatively dense, transparent liquid. A lesser density liquid was added by drops to titrate the *a*-C density. For dense resistive films, a 1,2,2,2 tetrabromoethane/ethanol mixture (a 98%/2% cocktail) with a density of 2.97 g/cm^3 was used to begin titrations. For low density conductive films, halothane 2-bromo, 2-chloro-1,1,1 triflouroethane, with a density of 1.87 g/cm^3, was used. Dry ethanol, miscible in both dense liquids, was used as the low-density (0.79 g/cm^3) titrating liquid. The density of liquid mixtures was determined by weighing pipetted solutions on an electronic balance with 100 μg resolution. Calibrations were made with flakes of bulk hot-pressed aluminum.

TABLE I. Columns one and two correlate labels $a-j$ used in Figs. 2(a)–5 with a-C deposition temperature. (N) designates films that were deposited with a beam neutralizer. The third column lists the range of the density of states at the Fermi level $N_V(E_F)$ extracted from fitting Eq. (4b) to the data sets and assuming $1\ \text{Å} < \alpha^{-1} < 10\ \text{Å}$.

Sample	$T_{\text{deposition}}$ (K)	Range of $N_V(E_F)$ ($\text{cm}^{-3}\,\text{eV}^{-1}$)
a	578	$1.2\times10^{20}-10^{23}$
$b(N)$	575	$7.0\times10^{19}-10^{22}$
c	465	$4.0\times10^{18}-10^{21}$
d	364	$3.8\times10^{18}-10^{21}$
e	350	$3.3\times10^{18}-10^{21}$
f	300	$1.8\times10^{18}-10^{21}$
g	272	$4.4\times10^{17}-10^{20}$
$h(N)$	373	$1.6\times10^{17}-10^{20}$
i	232	$2.8\times10^{17}-10^{20}$
$j(N)$	250	$3.4\times10^{16}-10^{19}$

The intrinsic stress of thin a-C films, deposited on one surface of silicon cantilever beams, was measured by observing the beam deflection induced by transmission of biaxial film stress across the carbon–silicon interface. Cantilevers were fabricated from small strips of polished, ultrathin silicon ⟨100⟩ membranes ranging from 25 to 125 μm thick, which were clamped at one end with 1 cm long regions extending across the central portion of the carbon ion beam. Beam deflections δ were concave downward and measured *ex situ* by noting the change in the plane of focus of the free end with an optical microscope. Resolution was approximately 2 μm for sub-mm scale deflections. Stress S was calculated for the a-C films by applying the limit of small deflection $\delta \ll l$ to approximate an assumed circular cantilever arc of radius $R \cong l^2/2\delta$ in the biaxial form of Stoney's equation, with the result,

$$S \cong \frac{E_Y t_S^2 \delta}{3(1-\nu) t l^2}. \tag{1}$$

E_Y is Young's modulus, ν Poisson's ratio, l the length, and t_S the thickness of the silicon beam.

III. EXPERIMENTAL RESULTS

A. Amorphous carbon conductivity

The first two columns of Table I list the deposition temperatures for 10 a-C films that were deposited with both neutralized (N) and non-neutralized beams. An Arrhenius plot shows the corresponding temperature dependence of the dc conductivities of the films as curves $a-j$ in Fig. 2(a). Both the dramatic increase of conductivity with increasing deposition temperature and the lower conductivity of films deposited with neutralized compared to non-neutralized beams are notable. As with other studies,[11] we found that heating the a-C above the deposition temperature irreversibly increased the conductivity. The magnitude of increase was greatest for the least conductive films, although the effect was always orders of magnitude less than that caused by heating films during deposition. The particular sensitivity of conductivity to deposition temperature compared to annealing temperature suggests that relaxation into conductive phase carbon proceeded most effectively near the surface of growing films rather than amongst constrained bulk atoms. Temperature excursions below the highest annealing temperature resulted in the repeatable data used in the following discussion.

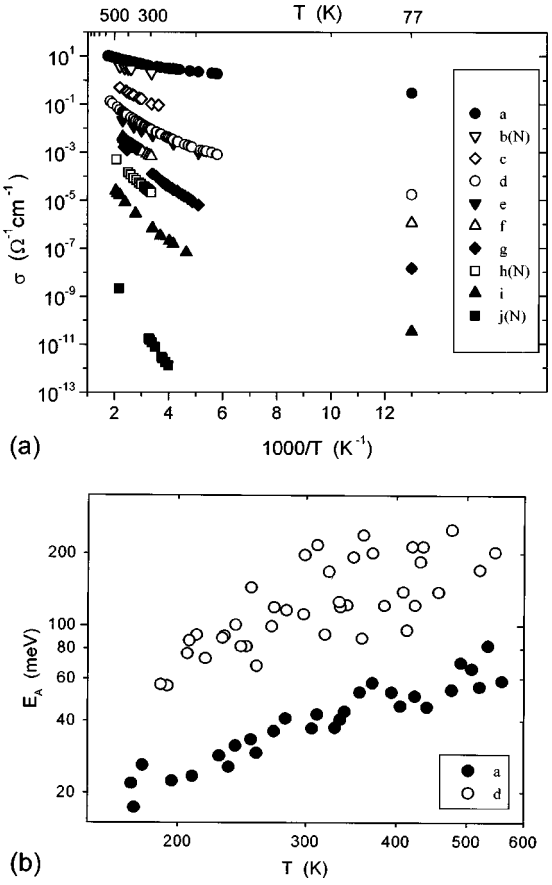

FIG. 2. (a) Arrhenius plot of the conductivities of 10 a-C films deposited on substrates held at the temperatures in Table I. (b) Double logarithmic plot of the temperature dependence of the differential activation energies $E_A(T)$ of films a and d.

During conductivity measurements, continuous current was applied and bias voltage assumed to be within a few percent of saturation as the temperature was decreased and data logged. Four point conductance was time dependent, with film bias voltage increasing slowly over hour-long time scales after reaching approximately 95% of saturation within minutes after current injection. Linear current versus saturation voltage curves were obtained for fields less than 10^4 V/m. Between 10^6 and 10^8 V/m, nonlinear current density versus voltage characteristics were obtained with $J \sim V^{1/2}$. We did not determine the extent to which field assisted transport or contact effects were responsible for this non-ohmic behavior. The time dependent conductivity data, the nonlinear current–voltage data, and the disordered structure of the material suggest that traps played an important role in conduction. A mechanism such as Frenkle–Poole emission[12] of carriers may therefore have controlled the field dependence of charge transport. Application of large electric fields through the planes of submicron thickness films caused irreversible increases in conductivity. No attempts were made to condition or burn in the electrode/film systems after

breakdown,[13] and all measurements were made well below the approximately 10^8 V/m damage threshold.

The effect of neutralization was most pronounced for insulating *a*-C deposited at low temperature, while conductive films deposited at high temperature were virtually unaffected by use of the neutralizer. The conductivities of films *a* and $b(N)$, deposited near 575 K differ by a factor of order 1. Yet the room-temperature conductivities of films *d* and $h(N)$ deposited near 370 K differ by three orders of magnitude, while films *i* and $j(N)$, deposited near 240 K, differ by nearly five orders of magnitude. By analogy to the observed high-field breakdown, these differences are attributed to growth of a conductive phase induced by dielectric breakdown of thin insulating films under internal electric fields generated by surface charging during depositions without a neutralizer. Possible explanations for the decreasing influence of neutralization on increasingly conductive films are the combined effects of the low internal electric fields and the likelihood of the presence of relatively stable sp^2 phase regions in conductive *a*-C.

The dominant contribution of nontetrahedrally bonded carbon to the optical and electronic properties of *a*-C is well established.[14] These unsaturated carbon atoms are expected to be localized in small clusters of a few atoms each, with sizes determined by competition between the thermally driven formation of π bonds and the densifying and disordering effects of ion impingement. Charge carriers are likely to be localized throughout the entire range of the sp^2 π, mixed valence, and dangling bond states within the band gaps associated with sp^2 and sp^3 σ bonds.[14] Furthermore, the small thermopower of conductive *a*-C indicates transport near the Fermi level rather than by activation across a wide mobility gap.[15] Therefore, conduction by tunneling or phonon assisted hopping between localized states, rather than through propagation in extended states, is expected throughout a broad range of temperatures for the *a*-C materials. A generalized conductivity sum,

$$\sigma(T)=\sum_i \sigma_{i0}(T)\exp\left[-\left(\frac{T_{i0}}{T}\right)^n\right], \tag{2}$$

with each term dominant in a different temperature range, can be fit to the data of Fig. 2(a). Each term models the contribution of a different charge transport processes, with $n=1$ applicable to nearest neighbor hopping or conduction in extended states, and $1/4\leqslant n\leqslant 1/2$ appropriate for hopping between localized states.[16] Numerical evaluation of the differential activation energies,

$$E_A(T)=-k_B\frac{\Delta \ln[\sigma(T)]}{\Delta(1/T)}, \tag{3}$$

for successive points in each data set shown in Fig. 2(a) results in a temperature dependent increase of the $E_A(T)$ as shown in Fig. 2(b) for data sets *a* and *d*. A single activated term with $n=1$ in Eq. (2) is therefore inadequate for modeling the conductivity throughout the temperature range spanned by the data. Although a few summed terms with different activation energies adequately fit the data, we avoid this approach because the lack of carrier density and mobility data introduces a set of loosely constrained fitting parameters. Further discussion is therefore focused on examination of the data in terms of phonon assisted hopping models.

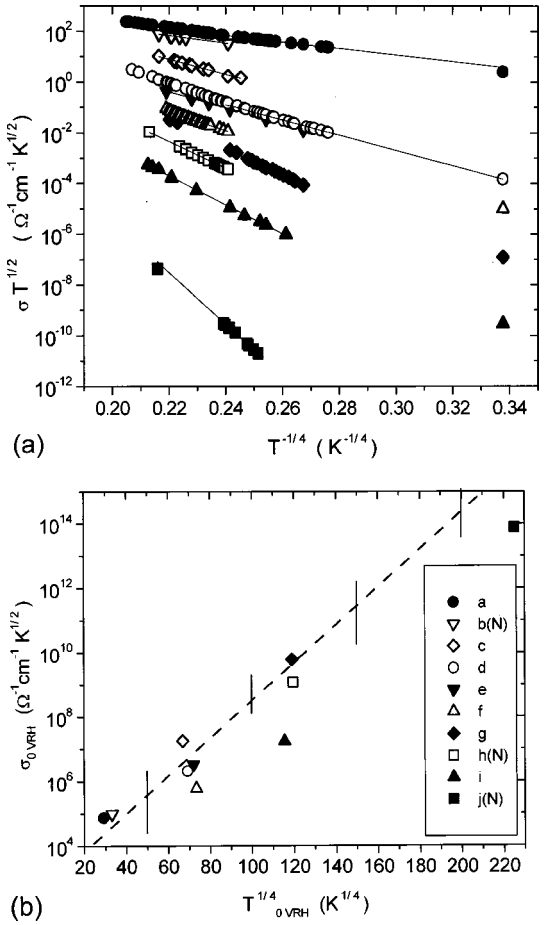

FIG. 3. (a) Conductivity data plotted in a form that linearizes Eqs. (4a) and (4b). The solid lines indicate the range of data used to extract values for $T_0^{1/4}$ and σ_0. (b) A plot of the variable range hopping parameters $T_0^{1/4}$ and $\sigma_{0\,\mathrm{VRH}}=T^{1/2}\,\sigma_0(T)$ for films $a-j$. For comparison, the dashed line corresponds to a linear fit to the $\sigma_{0\,\mathrm{VRH}}$ vs $T_0^{1/4}$ values found in Ref. 15, with the vertical bars indicating the local spreads of values.

Use of a single term in Eq. (2) to fit the conductivity data allows extraction of the range of fractional exponents $0.05\leqslant n\leqslant 0.5$ from the slope of data sets $a-j$ in Fig. 2(b).[15] The intermediate case of $n=1/4$ corresponds to conduction by single phonon assisted variable range hopping (VRH) of carriers in three dimensions, with[16]

$$\sigma_0(T)=e^2\nu_{\mathrm{ph}}\left(\frac{N_V(E_F)}{24\alpha k_B T}\right)^{1/2}, \tag{4a}$$

$$T_0^{1/4}=\left(\frac{24\alpha^3}{\pi k_B N_V(E_F)}\right)^{1/4}, \tag{4b}$$

where $N_V(E_F)$ is the VRH density of states at the Fermi level, α^{-1} the carrier localization length, and ν_{ph} a characteristic phonon frequency. The conductivity data are nearly linearized by the standard plotting of $\sigma T^{1/2}$ vs $T^{-1/4}$ in Fig. 3(a). Values for $T_0^{1/4}$ and $\sigma_{0\,\mathrm{VRH}}=T^{1/2}\sigma_0(T)$ were extracted from the curves shown as solid lines fit to the data sets over the low temperature range. These values are shown in Fig. 3(b) along with a summary of the results of the comprehensive analysis of a wide range of carbon materials from Ref.

15. As these authors discussed in detail, the increase of $\sigma_{0\,\mathrm{VRH}}$ with $T_0^{1/4}$ is precisely the opposite trend expected for the two quantities' reciprocal dependencies on $N_V(E_F)$ and α^{-1} in Eqs. (4). Further indication of the inappropriate form of these equations results from extraction of the density of states and carrier localization by simultaneous solution of Eqs. (4) for best fits to each of the data sets. As with other reports,[11,15,17] we find nonphysical values for both quantities, often with $N_V(E_F) \gg 10^{23}\,\mathrm{eV}^{-1}\,\mathrm{cm}^{-3}$ and $\alpha^{-1} < 1$ Å for the parameterized range $10^{11} < \nu_{\mathrm{ph}} < 10^{13}$ Hz. A further assumption that the localization length is associated with small sp^2 bonded clusters of a few atoms each allows setting $1\,\text{Å} < \alpha^{-1} < 10\,\text{Å}$ in Eq. (4b), yielding the reasonable range of values for the density of states $N_V(E_F)$ listed in Table I.

The multiphonon hopping model has been advanced to describe conduction in carbon materials ranging from insulating tetrahedral *a*-C and H:*a*-C to highly conducting evaporated carbon.[15,17] The conductivity is expressed in a form generally applicable to hopping transport[16] as

$$\sigma(T) = \tfrac{1}{6} N(E_F)(eR)^2 \Gamma(T), \tag{5}$$

with a hopping range R and rate $\Gamma(T)$. For carriers localized on the scale of a few lattice constants, with weak nonpolaronic lattice coupling, the temperature dependence of the conductivity is determined in the limit $k_B T \gg E_c$ by the multiphonon assisted hopping rate,

$$\Gamma(T) \sim C \exp(-\gamma m)(k_B T/E_c)^m. \tag{6}$$

The prefactor C is of the order ν_{ph}. A measure of the number of phonons participating in transport between hopping sites is given by $m = \Delta E/E_c$, with the ratio expressed as the average site energy difference ΔE (the zero phonon optical absorption energy) to the average energy E_c of the phonon modes coupled to the electrons. The electron–lattice coupling strength $E_m \cong E_S/2$, with E_S the Stokes shift, sets $\gamma \cong \ln(\Delta E/E_m) - 1$.[16] E_c has been associated with the energy $\hbar\omega_a$ of the acoustic phonon mode most effectively coupled to the electrons, where the frequency $\omega_a = \alpha a_0 \omega_m$ is reduced from the maximum ω_m by the ratio of carbon bond length a_0 to the localization length α^{-1}.[17] Alternatively, a constant E_c has also been proposed,[16] implying that phonon modes couple to the electronic states with efficiencies independent of the details of *a*-C microstructure.

Combination of Eqs. (5) and (6) yields the succinct expression $\sigma(T) = aT^m$. The double-logarithmic plot of Fig. 4(a) nearly linearizes the entire range of the *a*-C conductivity data, as expected from this model. Values for a and m, derived from the fitted curves, and representing an average over a range of phonon–charge carrier coupling strengths, are collected in Fig. 4(b) along with a summary of data from Ref. 15. A characteristic temperature Θ, associated with a common extrapolated conductivity for all data sets, was extracted from the slope of the fitted curve. Our data yield a common conductivity at $\Theta = 2700$ K, compared to 1500 K found in Ref. 15. While these temperatures are experimentally inaccessible, Θ is related to model parameters as $\gamma = \ln(\Theta/T_c)$.[15] $T_c = E_c/k_B$ has been estimated to be as low as 10 K, however, this resulted from setting a small α based on a localization scale determined by very large 60 Å cluster sizes and

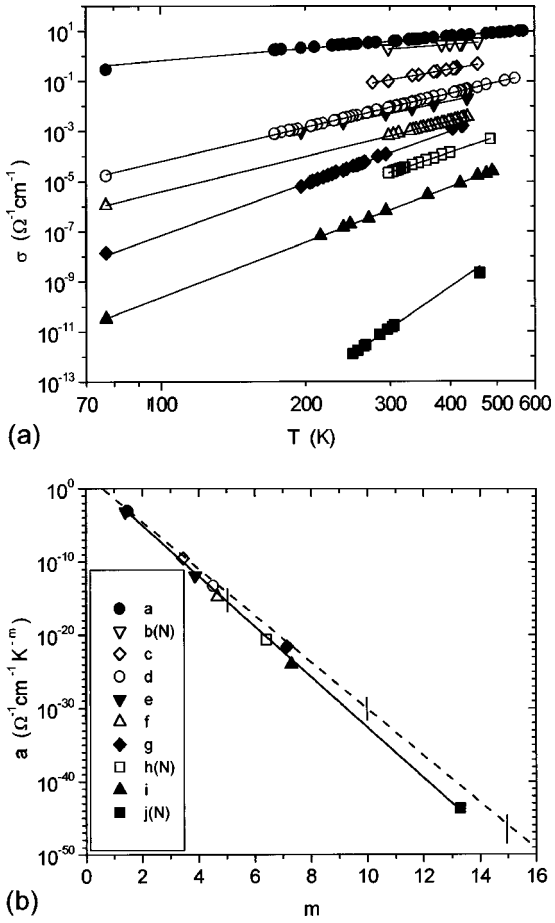

FIG. 4. (a) Double logarithmic plot of conductivity vs temperature. The solid lines are fits to the data using the form $\sigma(T) = \alpha T^m$. (b) Multiphonon parameters a and m extracted from the fitted curves in Fig. 4(a). The dashed line corresponds to a linear fit to the collection of *a*-C and H:*a*-C data of Ref. 15, with vertical bars indicating the local spread of values of a for three values of m.

using a relatively low Debye temperature of 390 K to set ω_m.[17] These values may be reasonable for conductive graphite-like *a*-C, however the large difference in Debye temperatures of graphite and diamond should produce a substantial variation in ω_m for the range of *a*-C materials. With structural models emphasizing the small size of sp^2 clusters in insulating *a*-C,[14] along with the likelihood of a range of localization lengths, the coupling strength could conceivably extend to $T_c > 100$ K if E_c depends on the microstructure. For $10\,\mathrm{K} < T_c < 100\,\mathrm{K}$, the data sets in Figs. 4(a) and 4(b) yield $3.3 < \gamma < 5.6$, and satisfy the weak coupling condition $(E_m/E_c)(k_B T/E_c) = m(T/T_c)e^{-(\gamma+1)} < 1$.[17]

B. Amorphous carbon stress and density

The bulk densities of *a*-C films deposited without a neutralizer are plotted versus deposition temperature in Fig. 5. The symbolic tags *a*, *c*, *d*, and *i* indicate that the conductivity data with the same labels in Figs. 2(a)–4(b) were taken for these films. The overall trend indicates decreasing *a*-C density with increasing deposition temperature. The primary measurement uncertainty in setting the end of density titrations was determining when the neutrally buoyant carbon

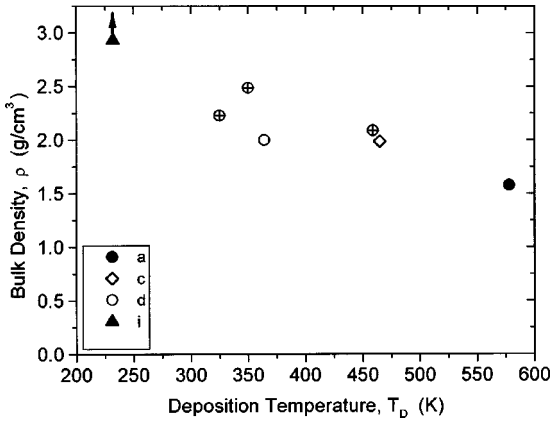

FIG. 5. Bulk density ρ of *a*-C films vs deposition temperatures for depositions made without a beam neutralizer. Symbols corresponding to the data of Figs. 2(a)–4(b) indicate that conductivity data was taken for the same film. The arrow indicates that the density of sample *i* exceeded 2.97 g/cm^3.

particles precipitated, resulting in approximately ± 0.05 g/cm^3 deviations in the measurements. Film stress is plotted in Fig. 6 versus deposition temperature determined by a thermocouple clamped at the beam base. Although some data were taken for films deposited alongside *a*-C for which conductivity data were obtained, the substrate temperatures differed substantially due to the poor thermal contact of the cantilever beam with the substrate holder. Because of the sensitive dependence of *a*-C properties on substrate temperature, no correspondence to other figures is implied. Variation of stress with film thickness was not investigated, however the nominally 0.1 μm thick films were considerably beyond the initial growth stage where variations in stress have been observed.[18] Systematic measurement errors in the intrinsic stress ranging up to ± 1 GPa were introduced by use of a macroscopic approximation to local curvature, neglect of the thermal stress component, variation of film thickness, and different formation temperatures over the length of the ~ 1 cm long beams. Control experiments of thermal cycling and sputtering of uncoated cantilevers produced no measurable deflections. Film stress resulted from both bond disorder and the differential thermal expansion of the silicon and carbon. The largest thermal stress component was estimated to be less than approximately 0.05 GPa.

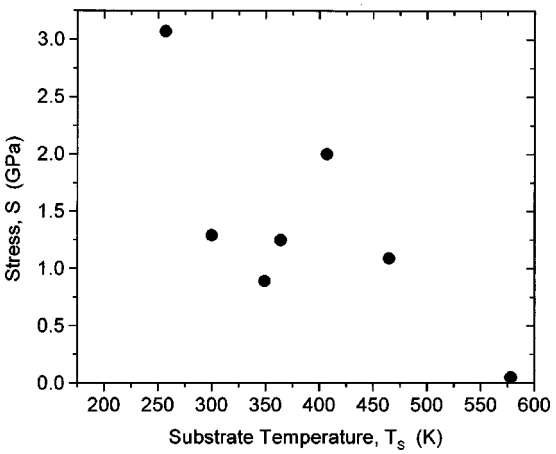

FIG. 6. Intrinsic stress *S* of *a*-C films vs deposition temperature for depositions made without a beam neutralizer.

IV. DISCUSSION

Computational simulations and deposition models have correlated carbon film formation processes with measurements of microstructure,[19] density,[19,20] stress,[18,21–24] and surface roughness.[25] The fundamental deposition parameters affecting the bulk and microstructural properties of amorphous carbon include the energy per deposited carbon atom, carbon flux, and substrate temperature. Because inference of microstructural details from bulk properties is speculative, we relate our *a*-C conductivity, stress, and density data to sp^2 and sp^3 hybridizations of carbon atoms in only the most general terms. A number of experiments at fixed substrate temperature utilized mass filtered beams to investigate the influences of incident ion energy and flux.[18,20] In these studies, decreasing stress and density were correlated with measurements of increasing fractions of sp^2 bonds. One model of the amorphous carbon pressure-temperature (PT) phase plane replaces the sharp Bermann–Simon delineation of crystalline sp^2 and sp^3 carbon stability with a continuous gradation from amorphous sp^2 to sp^3 bonding with increasing pressure.[18] In the context of this model, our series of *a*-C depositions correspond to a traversal of the graded amorphous sp^2–sp^3 carbon PT phase region towards increasing bulk fraction of sp^2 bonded carbon with increasing deposition temperatures. The fixed 300 eV beam energy resulted in an approximate partition of 50–300 eV per carbon atom in the molecular ions. With fixed flux and substrate temperature, the range of atomic impact energies resulted in a range of film stresses reflecting the local formation temperatures and pressures.[18,20,22,23]

Although the sp^2 bonded phase is thermodynamically favored at high temperatures, sp^2 π bonded cluster growth is hindered by the disordering effects of ion impacts.[14] The dramatic increase of *a*-C conductivity with increasing deposition temperature may be an indirect indication of growth of the sp^2 π bonded carbon volume fraction. We expect that the balance between equilibrium and nonequilibrium formation processes favors increasing π bonded cluster sizes with increasing deposition temperature. The density of free carriers would increase with delocalization of sp^2 and sp^3 states, and both the carrier localization length α^{-1} and the distance *R* between localized states would be reduced with increasing cluster sizes. An exponential increase in the magnitude of conductivity would thereby result from the factor $\exp(-2\alpha R)$ implicit in Eqs. (2), (4), and (5), which arises from the dependence of the transition rate on the overlap integrals of the localized wave functions.[16]

A description of the *a*-C conductivity by activated transport processes requires up to three terms in Eq. (2) to fit data over the temperature range spanning from 77 to 600 K. Multiple activated terms could correspond to an increasing thermal energy scale that successively promotes carriers from conduction at the Fermi level into higher ranges of localized and then extended states. Because of the large numbers of

parameters required for such fitting, the continuous increase in $E_A(T)$ shown in Fig. 2(b), the likelihood of hopping transport near the Fermi level,[15] and a deep mobility edge,[14] we did not pursue this approach. Single phonon assisted variable range hopping also seems untenable as a conductivity mechanism for the range of *a*-C films because of the nonphysical values for quantities extracted from fits of conductivity data in the low temperature range and the inverse correlation of $\sigma_{0\,\mathrm{VRH}}$ with $T_0^{1/4}$. Nonetheless, fixing the localization length α^{-1} in Eq. (4b) allowed extraction of the reasonable range of values for $N_V(E_F)$ displayed in Table I. Furthermore, with the demarcation between high and low temperature transport process set at approximately half the Debye temperature, features such as VRH ordinarily associated with low temperatures could persist above room temperature in *a*-C containing substantial quantities of sp^3 bonded phase. The steadily increasing values of $E_A(T)$ shown in Fig. 2(b) indicate that no transformation to nearest neighbor hopping, with $n=1$ and $E_A(T)$ converging to the average site difference energy,[16] was found for temperatures less than 600 K. Caveats regarding application of the multiphonon hopping model to *a*-C notwithstanding,[15] the power law temperature dependence of $\sigma(T)\sim T^m$ of Eq. (6), resulting from the $k_BT \gg E_c$ limit of a product of m Bose phonon occupation factors, fits the form of our *a*-C conductivity data well. In this model, the primary factor governing the magnitude of conductivity at fixed temperature is the hopping rate's exponential dependence on the number of participating phonons m with $\Gamma\sim(T_c e^{\gamma})^{-m}$. The hopping rate Γ can be correlated to the *a*-C microstructure in a model of sp^2 states localized to small clusters whose number density, separation R, size α^{-1}, and intracluster order are set by deposition conditions. These parameters determine the coupling strength E_c and the average energy ΔE required for a charge carrier hop.

V. CONCLUSION

Fullerenes were used as a pure carbon feedstock in our specially constructed ion source to deposit amorphous carbon films with widely ranging conductivities, densities, and stresses. The unique feature of our method for producing *a*-C was the exclusive use of a high vapor pressure solid state source to supply a pure carbon discharge in a gridded ion gun. This insured process purity, allowed independent control of ion energy and beam flux, and provided a means for covering large area, low-temperature, insulating substrates. We have shown that the conductivity of *a*-C films depends critically on the substrate temperature and beam neutralization. Irreversible changes in *a*-C conductivity resulted from imposition of electric fields exceeding 10^8 V/m and from annealing films at temperatures higher than the deposition temperature. The microstructure of our *a*-C films was not determined, however consideration of the increased phase stability of sp^2 π bonded carbon with increasing temperature provides consistent explanations for the trends of decreasing stress, density, and resistivity observed for increasing deposition temperatures. Although different charge transport processes could dominate conductivity in different temperature ranges, the form of the conduction was well modeled by a single term with a power law temperature dependence characteristic of conduction by multiphonon assisted hopping.

ACKNOWLEDGMENTS

The authors thank M. Ata of the Sony Corporation Frontier Science Laboratory for photoelectron spectroscopy data. They are grateful for the donation of silicon membranes by Virginia Semiconductor, Inc. and high-purity graphite by Poco Graphite, Inc.

[1] D. M. Gruen, Nucl. Instrum. Methods Phys. Res. B **78**, 118 (1993).
[2] H. Gaber, H.-G. Busmann, R. Hiss, I. V. Hertel, H. Romberg, J. Fink, F. Bruder, and R. Brenn, J. Phys. Chem. **97**, 8244 (1993).
[3] E. B. Maiken and P. Taborek, J. Appl. Phys. **78**, 541 (1995).
[4] E. B. Maiken and P. Taborek, *Applications of Diamond Films and Related Materials*, NIST Special Publication No. 885, 1995, edited by A. Feldman, p. 719.
[5] V. Paillard, P. Melinon, V. Dupuis, J. P. Perez, A. Perez, and B. Champagnon, Phys. Rev. Lett. **71**, 4170 (1993).
[6] P. D. Horak and U. J. Gibson, Appl. Phys. Lett. **65**, 968 (1994).
[7] Z. Ren, X. Xiong, Y. Du, Z. Ying, F. Li, and L. Chen, J. Appl. Phys. **77**, 4142 (1995).
[8] D. M. Gruen, S. Liu, A. R. Krauss, J. Luo, and X. Pan, Appl. Phys. Lett. **64**, 1502 (1994).
[9] We refer broadly to amorphous carbon materials deposited by a variety of techniques, with bond types and physical characteristics ranging from hard, resistive diamond-like to conductive, graphite-like materials as *a*-C.
[10] Some beam neutralization occurred by the trapping of electrons ejected from the *a*-C surface or from background gas.
[11] D. Dasgupta, F. Demichelis, and A. Taglaferro, Philos. Mag. B **63**, 1255 (1991).
[12] C. Ronning, U. Griesmeier, M. Gross, H. C. Hofsass, R. G. Downing, and G. P. Lamaze, Diamond Relat. Mater. **4**, 666 (1995).
[13] M. M. Freeman, A. L. Barton, and H. L. Marcus, *Applications of Diamond Films and Related Materials*, NIST Special Publication No. 885, 1995, edited by A. Feldman, p. 785.
[14] J. Robertson, Philos. Mag. B **76**, 335 (1997).
[15] A. Helmbold, P. Hammer, J. U. Thiele, K. Rohwer, and D. Meissner, Philos. Mag. B **72**, 335 (1995).
[16] N. F. Mott and E. A. Davis, *Electronic Processes in Non-crystalline Materials*, 2nd ed. (Oxford University Press, Oxford, 1979).
[17] K. Shimakawa and K. Miyake, Phys. Rev. B **39**, 7578 (1989).
[18] D. R. McKenzie, J. Vac. Sci. Technol. B **11**, 1925 (1993).
[19] P. J. Fallon, V. S. Veerasamy, C. A. Davis, J. Robertson, G. A. J. Amaratunga, W. I. Milne, and J. Koskinen, Phys. Rev. B **48**, 4777 (1993).
[20] C. A. Davis, Thin Solid Films **226**, 30 (1993).
[21] J. Robertson, J. Non-Cryst. Solids **164–166**, 1115 (1993).
[22] Y. Yin and D. R. McKenzie, Thin Solid Films **280**, 95 (1996).
[23] D. R. McKenzie, D. Muller, and B. A. Pailthorpe, Phys. Rev. Lett. **67**, 773 (1991).
[24] Y. Lifshitz, G. D. Lempert, and E. Grossman, Phys. Rev. Lett. **72**, 2753 (1994).
[25] Y. Lifshitz, S. R. Kasi, J. W. Rabalais, and W. Eckstein, Phys. Rev. B **41**, 10468 (1990).